

## Fluorescent Probes

How to cite: *Angew. Chem. Int. Ed.* **2020**, *59*, 15152–15156

International Edition: doi.org/10.1002/anie.202004142

German Edition: doi.org/10.1002/ange.202004142

## Real-Time In Vivo Detection of Cellular Senescence through the Controlled Release of the NIR Fluorescent Dye Nile Blue

Beatriz Lozano-Torres<sup>+</sup>, Juan F. Blandez<sup>+</sup>, Irene Galiana, Alba García-Fernández, María Alfonso, María D. Marcos, Mar Orzáez, Félix Sancenón,\* and Ramón Martínez-Máñez\*

**Abstract:** *In vivo* detection of cellular senescence is accomplished by using mesoporous silica nanoparticles loaded with the NIR-FDA approved Nile blue (NB) dye and capped with a galactohexasaccharide (S3). NB emission at 672 nm is highly quenched inside S3, yet a remarkable emission enhancement is observed upon cap hydrolysis in the presence of  $\beta$ -galactosidase and dye release. The efficacy of the probe to detect cellular senescence is tested *in vitro* in melanoma SK-Mel-103 and breast cancer 4T1 cells and *in vivo* in pablociclib-treated BALB/cByJ mice bearing breast cancer tumor.

Cellular senescence is a stable state of cell cycle arrest necessary for maintaining the organism homeostasis.<sup>[1]</sup> However, the improper elimination of senescent cells provokes local inflammation, tissue degeneration and contributes to aging.<sup>[2]</sup> Evidence supports that accumulation of senescent cells is involved in the pathophysiology of many age-related diseases<sup>[3]</sup> and has boosted the concept that senescent cells are an attractive therapeutic target.<sup>[4,5]</sup> Recent reports, using *in vivo* models, indicate that a wide variety of diseases can be ameliorated by the elimination of senescent cells.<sup>[6,7]</sup>

Characteristic signs of cellular senescence include changes in cell morphology,<sup>[8]</sup> the appearance of condensed nuclear chromatin foci, known as senescence-associated heterochromatic foci (SAHF),<sup>[9]</sup> and the overexpression or activation of tumor suppressor proteins such as p53, p16<sup>INK4a</sup>, and p21 that contribute to cell cycle arrest.<sup>[10]</sup> Moreover, one of the most widely used markers to detect cellular senescence is the overexpression of lysosomal  $\beta$ -galactosidase, also referred to as senescence-associated  $\beta$ -galactosidase (SA- $\beta$ -Gal).<sup>[11]</sup> Measurement of SA- $\beta$ -Gal activity using chromo-fluorogenic probes has become popular as an easy and simple procedure to detect senescence.<sup>[12,13]</sup> The use of molecularly imprinted nanoparticles has also been described recently for senescence detection.<sup>[14,15]</sup> However, most of the actual probes are suitable for *in vitro* studies, whereas probes to detect cellular senescence *in vivo* in realistic senescence models are scarce. One general drawback of most of these probes is that, even in realistic senescence models, detection is only possible after the animal sacrifice. Consequently, the development of suitable methods for *in vivo* senescence detection remains an unresolved problem.<sup>[2]</sup>

Based on the above, we report the use of nanoparticles<sup>[16]</sup> for *in vivo* detection of cellular senescence using a NIR fluorophore. The probe consists of galactohexasaccharide-capped mesoporous silica nanoparticles (MSNs), which are able to release their cargo in senescent cells due to the hydrolysis of the capping oligosaccharide by SA- $\beta$ -Gal.<sup>[17]</sup> We tested a number of fluorophores as cargo and finally selected Nile blue (NB) due to its remarkable features as *in vivo* imaging agent. NB is an organic dye approved by the Food and Drug Administration (FDA) for human use<sup>[18]</sup> and it exhibits near-infrared emission at 672 nm.<sup>[19,20]</sup> Most importantly, NB is an aromatic planar fluorophore, which is highly quenched at high concentrations or in confined spaces as it forms non-emissive  $\pi$ -stacked aggregates.<sup>[21]</sup>

MSNs have been widely used as drug delivery systems due to their properties, such as biocompatibility and easy functionalization.<sup>[22]</sup> In addition to MSNs, other carriers for cargo delivery such as liposomes, micelles, and polymers have also been used in recent years.<sup>[23]</sup> In our case, MSNs were chosen as nanocarriers due to their high loading capacity, allowing the NB dye to be entrapped at high concentration resulting in effective dye–dye  $\pi$ -stacking interactions and quenching. This compact packaging together with the gating capability exerted by the capping galactohexasaccharide (see below) could not be obtained using other nanocarriers. In fact, MSNs are well suited for the preparation of on-demand delivery carriers by the functionalization of the outer surface with (bio)molecules that prevent payload release unless exposed

[\*] B. Lozano-Torres,<sup>[+]</sup> Dr. J. F. Blandez,<sup>[+]</sup> I. Galiana, Dr. M. Alfonso, Prof. M. D. Marcos, Dr. F. Sancenón, Prof. R. Martínez-Máñez Instituto Interuniversitario de Investigación de Reconocimiento Molecular y Desarrollo Tecnológico (IDM), Universitat Politècnica de València, Universitat de València Camino de Vera s/n, 46022 Valencia (Spain) E-mail: fsancenon@upvnet.upv.es rmaez@qim.upv.es

B. Lozano-Torres,<sup>[+]</sup> Dr. J. F. Blandez,<sup>[+]</sup> I. Galiana, Prof. M. D. Marcos, Dr. M. Orzáez, Dr. F. Sancenón, Prof. R. Martínez-Máñez Unidad Mixta UPV-CIPF de Investigación en Mecanismos de Enfermedades y Nanomedicina, Universitat Politècnica de València, Centro de Investigación Príncipe Felipe, Valencia (Spain)

B. Lozano-Torres,<sup>[+]</sup> A. García-Fernández, Prof. M. D. Marcos, Dr. F. Sancenón, Prof. R. Martínez-Máñez CIBER de Bioingeniería, Biomateriales y Nanomedicina (CIBER-BBN) (Spain)

B. Lozano-Torres,<sup>[+]</sup> Dr. J. F. Blandez,<sup>[+]</sup> Prof. M. D. Marcos, Dr. F. Sancenón, Prof. R. Martínez-Máñez Unidad Mixta de Investigación en Nanomedicina y Sensores Universitat Politècnica de València, IIS La Fe, Valencia (Spain) Dr. M. Orzáez Centro de Investigación Príncipe Felipe Eduardo Primo Yúfera, 3, 46012 Valencia (Spain)

[+] These authors contributed equally to this work.

Supporting information and the ORCID identification number(s) for the author(s) of this article can be found under: <https://doi.org/10.1002/anie.202004142>.

to specific stimuli.<sup>[23]</sup> Moreover, in MSN the cargo is simply encapsulated, while in some other nanoparticles cargo molecules need to be covalently linked.

The prepared nanoparticles (i.e., **S3** in Figure 1) are therefore poorly emissive, yet SA- $\beta$ -Gal-induced hydrolysis of the capping hexagalacto-saccharide to give galactose residues is expected to result in NB release, selectively inducing a marked NIR emission enhancement in senescent cells. Targeting of senescent cells in vitro with **S3** is validated in SK-Mel-103 (human melanoma) and 4T1 (murine breast cancer) cell lines treated with palbociclib. Moreover, in vivo detection of cellular senescence is demonstrated in BALB/cByJ mice bearing breast cancer tumor treated with senescence-inducing chemotherapy.

**S3** is easily prepared from mesoporous silica nanoparticles,<sup>[24]</sup> which are loaded with NB, externally functionalized with APTES and finally capped with  $\beta$ (1,4)-hexagalacto-saccharide (Supporting Information, Scheme S1). The mesoporous structure in **S3** and the starting mesoporous silica material (**S0**) was clearly observed by HR-TEM (Figure 2 a,b and Figure S1a) and by powder X-ray diffraction (Figure S1b). **S3** was also characterized by porosimetry (Figure S2a,b and Table S1), attenuated total reflectance (ATR, Figure S3), and dynamic light scattering (DLS, Figure S4). Moreover, from dye delivery experiments and thermogravimetric studies, the content of NB in **S3** was determined to be 0.45 mmol per gram of solid (Figure S5).

Quenching of NB inside the pores of **S3** was assessed. Free NB solutions presented much higher fluorescence than suspensions of **S3**, which showed negligible emission at

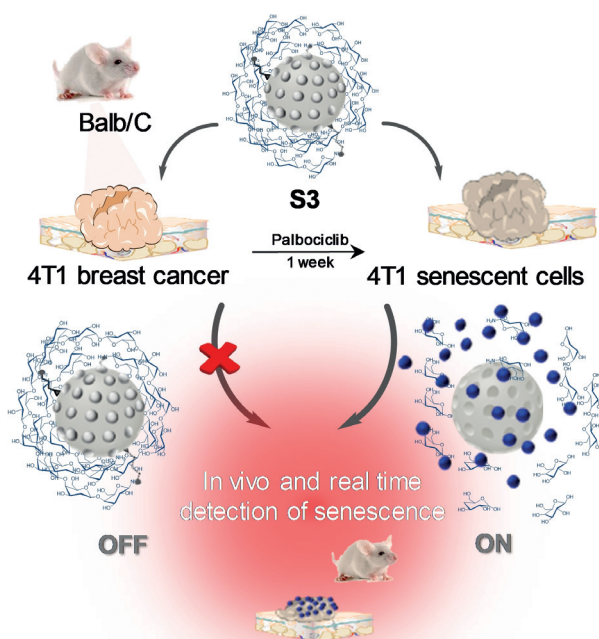


**Figure 1.** Representation of **S3** activation in BALB/cByJ female mice orthotopically injected with 4T1 cells to generate breast tumors. After tumor formation, mice were administered with palbociclib to generate senescence and treated with **S3** achieving in vivo detection of cellular senescence.

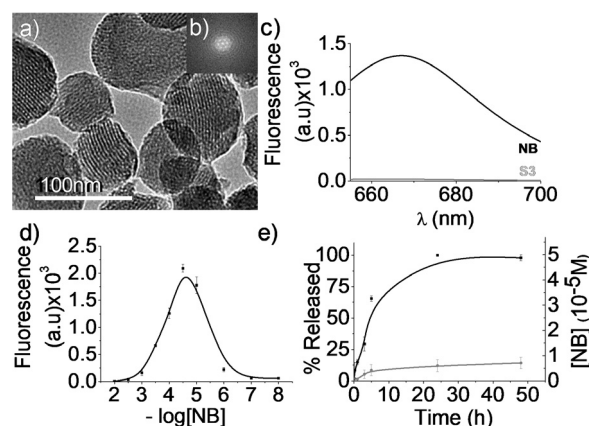


**Figure 2.** a) HR-TEM images of **S3**, b) TEM-EDX of **S3**. c) Fluorescence of a NB solution ( $1.81 \times 10^{-4}$  M) and of **S3** suspensions at equivalent concentrations of the dye. d) Emission intensity of NB solutions vs. fluorophore concentration. e) Release profile of **S3** in the absence (grey line) and in the presence of  $\beta$ -Gal (black line). Experiments were carried out in water/DMSO 99:1 v/v mixtures at pH 4.5. Error bars are expressed as  $3\sigma$ .

equivalent NB concentrations (Figure 2c). Moreover, confocal images of **S3** demonstrated that capped nanoparticles were poorly emissive (Figure S6). Quenching of NB at high concentrations was also studied in solution by monitoring the emission of the fluorophore at 666 nm ( $\lambda_{exc} = 635$  nm) at different NB concentrations in water (pH 4.5)/DMSO 99:1 v/v mixtures. Emission of the NB solutions increased until a concentration of circa  $1.0 \times 10^{-4}$  M, whereas at higher concentrations the fluorescence decreased. In fact, NB concentrations higher than  $10^{-3}$  M are poorly emissive (Figure 2d). From the amount of NB loaded and the specific pore volume in **S3** a molar concentration of the dye in the pores of circa 0.49 M was calculated, which is in agreement with the low emission observed for **S3** in Figure 2c.

Delivery of NB from **S3** was studied in the presence and absence of  $\beta$ -Gal (Figure 2e). **S3** show a marked NB delivery in the presence of  $\beta$ -Gal of circa 90% of the maximum dye released after 24 h, which corresponded to 31.4% ( $5.69 \times 10^{-5}$  M) of the dye entrapped (Figure S7). In contrast, a low NB release in the absence of  $\beta$ -Gal was found. Release in the presence of  $\beta$ -Gal is due to the hydrolysis of glycosidic bonds in the capping galacto-saccharide, which reduced steric crowding around the pores allowing NB delivery.

Specific targeting of senescent cells in vitro with **S3** was demonstrated in SK-Mel-103 (human melanoma) and 4T1 (murine breast cancer) cells treated with  $5 \mu\text{M}$  palbociclib (a CDK4/6 inhibitor, which suppresses DNA replication inducing cell cycle arrest) for two weeks to induce senescence. Senescence was confirmed by X-Gal staining (Figure 3 a,e,i,m).

Confocal microscopy studies of palbociclib-treated SK-Mel-103 and 4T1 cells, incubated with **S3**, revealed an intense fluorescent signal (Figure 3 g,o), whereas non-senescent SK-Mel-103 and 4T1 cells treated with **S3** presented weak fluorescence (Figure 3 c,k). Both control and senescent SK-Mel-103 and 4T1 cells showed also negligible background (Figure 3 b,f,j,n). In addition, it was found that control and

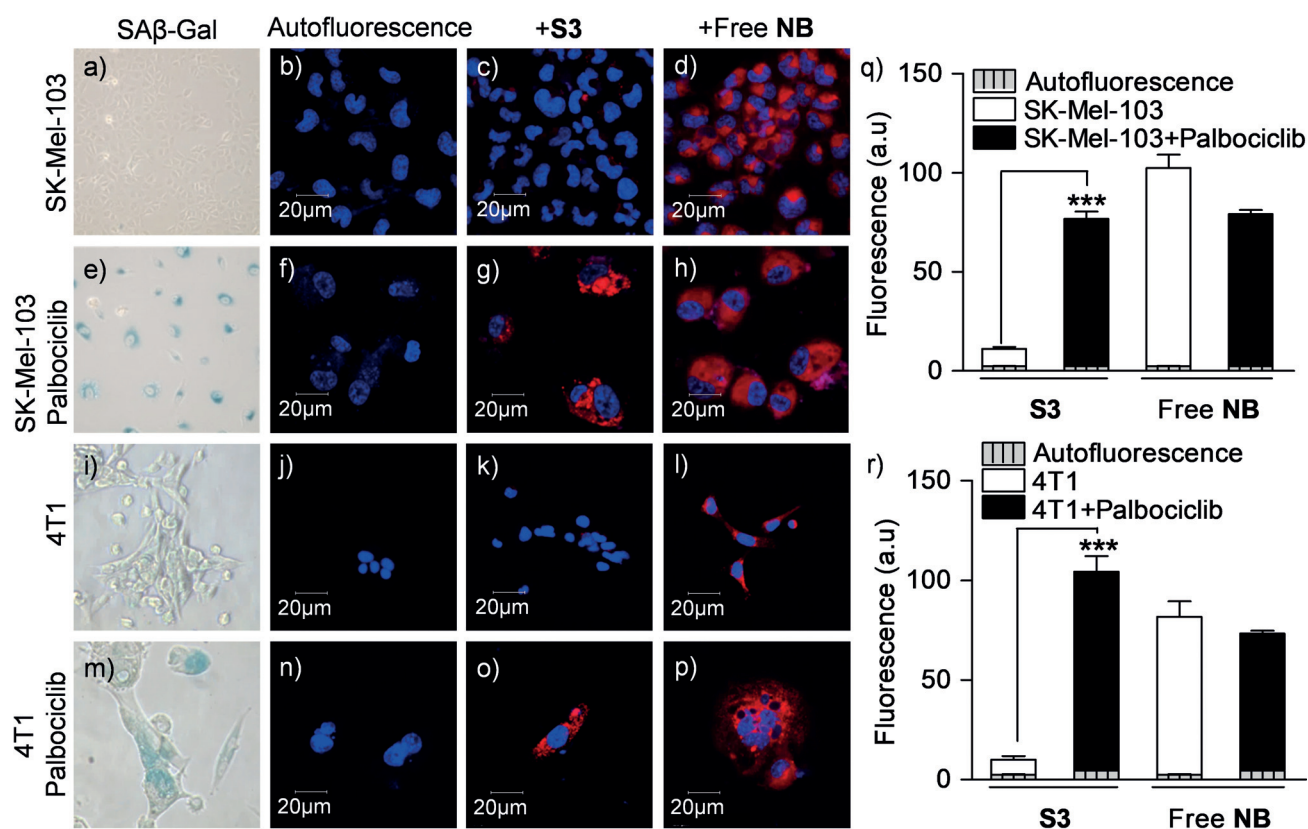


**Figure 3.** a, e, i, m) X-Gal assay for detection of SA-β-Gal expression in (a) control and (e) senescent SK-Mel-103 cells and in (i) control 4T1 and (m) senescent 4T1 cells. b, c) Confocal images of control SK-Mel-103 cells (b) in the absence or (c) in the presence of **S3**. f, g) SK-Mel-103 cells treated with palbociclib (f) in the absence (g) or in the presence of **S3**. d, h) Confocal images of (d) control SK-Mel-103 cells or (h) SK-Mel-103 cells treated with palbociclib in the presence of equivalent doses of free **NB**. j, k) Confocal images of control 4T1 cells (j) in the absence or (k) in the presence of **S3**. n, o) 4T1 cells treated with palbociclib (n) in the absence (o) or in the presence of **S3**. l, p) Confocal images of (l) control 4T1 cells or (p) 4T1 treated with palbociclib in the presence of equivalent doses of free **NB**. Cells were incubated with **S3** ( $7.8 \mu\text{g mL}^{-1}$ ) for 4.5 h in DMEM (10% FBS) in 20%  $\text{O}_2$  and 5%  $\text{CO}_2$  at 37°C, washed three times and stained with Hoechst ( $1.5 \text{ ng mL}^{-1}$ ) for 15 min. Representative images from repeated experiments ( $n=3$ ) are shown. q) Fluorescence emission of released **NB** in control and palbociclib-treated SK-Mel-103 cells incubated with **S3** and upon treatment with equivalent doses of free **NB**. Autofluorescence is the emission observed in SK-Mel-103 cells without treatment with **S3** or free **NB**. r) Fluorescence emission of released **NB** in control and palbociclib-treated 4T1 cells incubated with **S3** and upon treatment with equivalent doses of free **NB**. Autofluorescence is the emission observed in 4T1 cells without treatment with **S3** or free **NB**. Error bars represent s.d.

senescent cells treated with equivalent doses of free **NB** presented nearly the same fluorescence (Figures 3d, h, l, p, see also Figure S8). Quantification of fluorescence showed 7-fold emission enhancement in senescent SK-Mel-103 cells treated with **S3** compared to controls (Figure 3q). For the 4T1 cell line, the emission enhancement of senescent cells treated with **S3** when compared to control 4T1 cells was 10-fold. Results are indicative of **S3** uptake and galacto-oligosaccharide hydrolysis by SA-β-Gal in senescent cells, resulting in **NB** release. Moreover, it was found that **S3** nanoparticles were not toxic for both control and senescent cells (Figure S9).

In vivo detection of cellular senescence with **S3** was validated in mice bearing breast tumors treated with senescence-inducing chemotherapy. For this purpose, BALB/cByJ female mice were orthotopically injected with 4T1 (mouse mammary carcinoma) cells ( $0.5 \times 10^6$  cells mouse $^{-1}$ ) to generate breast tumors.

Mice were divided into four groups, control individuals with 4T1 tumors (A), control individuals with 4T1 tumors administered with **S3** (B), mice only administered with

palbociclib (C), and individuals with 4T1 tumors treated with palbociclib and **S3** (D). Groups C and D were treated daily by oral gavage with palbociclib after tumor development to induce senescence and arrest of tumor growth. After 7 days of palbociclib treatment, **S3** nanoparticles were intravenously administered to groups B and D, and mice were monitored by an in vivo imaging system (IVIS) at different time points for 48 h. No autofluorescence was observed from control (A) and palbociclib (C) treated mice (Figure S10). Mice from groups A, B, and C showed negligible fluorescence in the tumor area, while a strong fluorescent signal was observed for group D, which was administered both with palbociclib and **S3** (Figure 4a). The peak of maximum fluorescence in mice treated with palbociclib and **S3** (group D) was observed 24–36 h post-injection of the nanoparticles (Figure 4a), whereas a clear decrease in the fluorescence signal was found at 48 h. Quantification of the relative values of radiance ( $\text{p/s/cm}^2/\text{sr} \times 10^{10}$ ) showed an enhancement of 4.3-fold at 24 h and 7.3-fold at 36 h in palbociclib + **S3** treated mice when compared to mice treated with vehicle + **S3** (Figure 4b).

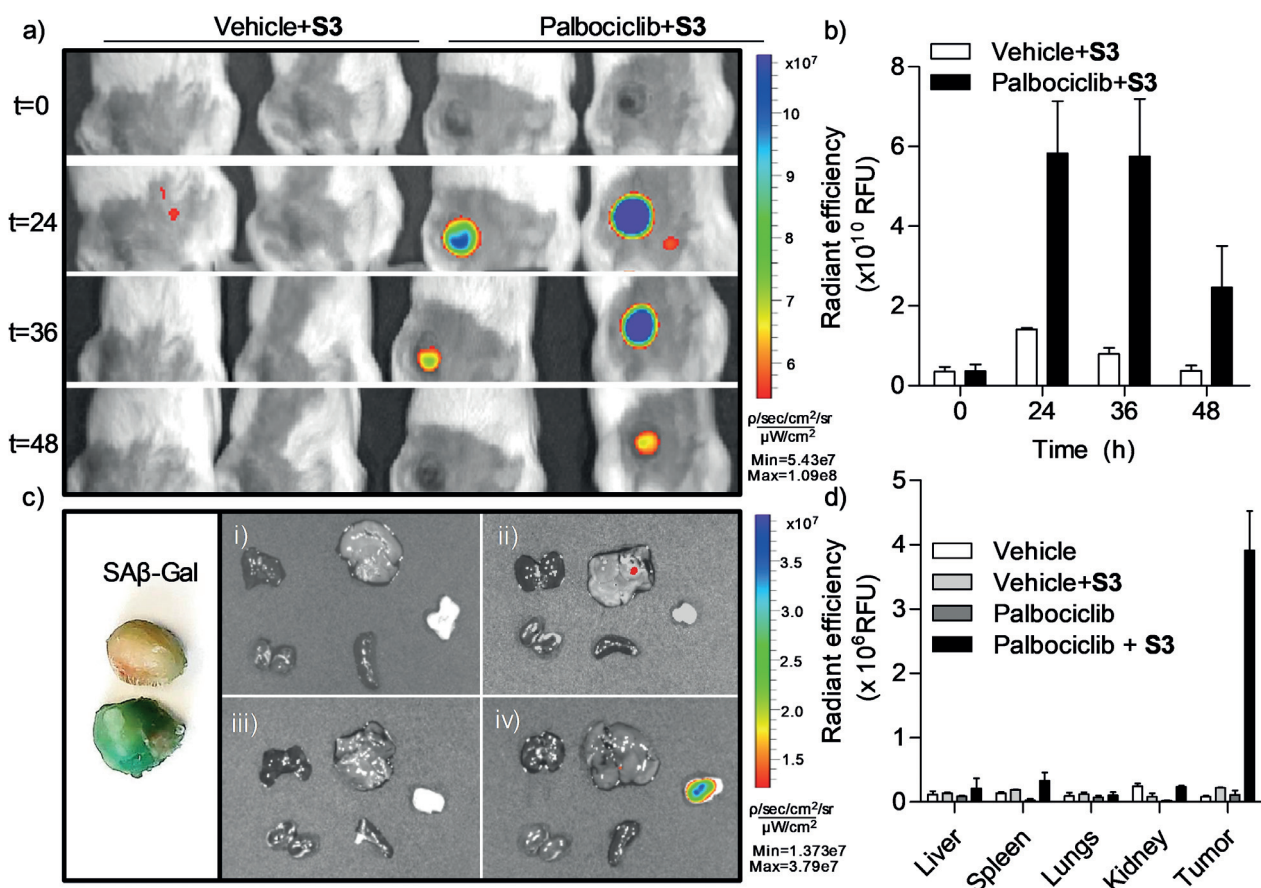


**Figure 4.** a) IVIS images at different time points of BALB/cBy female mice bearing 4T1 breast tumor. From left to right control mice treated with **S3** (two mice from group B) and BALB/cBy mice treated by oral gavage with palbociclib (senescent tumors) for 1 week and intravenously injected with **S3** (two mice from group D). b) Fluorescence emission intensity from tumor signals with time. Error bars represent s.d. c) X-Gal assay for SA- $\beta$ -Gal expression in tumors from control group A (top) and palbociclib-treated group C (bottom). IVIS images of organs and tumors from BALB/cBy female mice bearing 4T1 breast tumor. From left to right and from top to bottom: lungs, liver, tumor, kidney and spleen. (i) Control mice (group A). (ii) Control mice treated with **S3** (group B, 4 mg mL<sup>-1</sup> 200  $\mu$ L). (iii) BALB/cBy female mice bearing 4T1 breast tumor treated oral gavage with palbociclib for 1 week (group C). (iv) Palbociclib-treated mice intravenously injected with **S3** (group D, 4 mg mL<sup>-1</sup> 200  $\mu$ L). Mice were sacrificed 24 h post-treatment for these images. d) Fluorescence emission from organs and tumors in (i–iv). Error bars represent s.d.

Mice were euthanized and blood, lungs, liver, kidney, spleen, and tumors were ex vivo analyzed. Senescence in tumors from mice treated with palbociclib was confirmed by X-Gal staining (Figure 4c) and reduced immunostaining of the Ki67 proliferation marker indicative of cell cycle arrest (Figure S11). IVIS images of excised organs and tumors from vehicle (A) or palbociclib-treated mice (C) did not show any fluorescence (Figures 4c, i and iii). Similarly, tumors from vehicle-treated mice injected with **S3** (B) did not show any noticeable fluorescent signal (Figure 4c, ii). In contrast, strong emission (ca. 17.6-fold) was observed in tumors from mice treated with palbociclib and intravenously injected with **S3** (Figure 4c, iv and Figure 4d). Biodistribution of nanoparticles was studied by determining silicon levels in various organs by inductively coupled plasma mass spectroscopy (ICP-MS) (Figure S12). Nanoparticles reach both senescent and non-senescent tumors at 24 h, whereas levels of Si are significantly reduced 48 h post-injection, which is consistent with the patterns of fluorescence signal (see before). **S3** also accumulated in spleen, lungs and kidney at 24 h, whereas maximum silicon accumulation was found in the spleen at 48 h. Note that even though some MSNs accumulate in the

liver, spleen or kidney, negligible fluorescence was detected in these organs 24 h post injection. This is due to the very low emission from the capped **S3** (due to  $\pi$ -stacking NB interactions in the pores) and also indicates that nanoparticles remain capped in these organs, which did not overexpress SA- $\beta$ -Gal enzyme. Blood biochemistry and hematology analysis of different parameters, such as albumin (ALB), bilirubin (BIL), alkaline phosphatase (AKP), glutamic pyruvic transaminase (GPT), and aspartate transaminase (GOT), showed no signs of organ damage and systemic inflammatory response after MSN administration (B and D) when compared to **S3** untreated (A and C) groups (Figure S13).

In summary, we have described MSNs loaded with NB dye and capped with a galacto-oligosaccharide for the in vivo detection of cellular senescence. **S3** nanoparticles are poorly emissive due to  $\pi$ -stacking interactions of NB molecules densely packed onto the mesopores, yet NB is selectively released in senescent cells resulting in a marked emission enhancement. In vitro targeting of senescent cells with **S3** was validated in SK-Mel-103 and 4T1 cells treated with palbociclib. A remarkable enhanced emission in palbociclib-treated SK-Mel-103 and 4T1 senescent cells was observed when

incubated with **S3** in comparison with control cells. **S3** was validated in vivo in BALB/cByJ female mice orthotopically injected with 4T1 cells to generate breast tumors and treated with palbociclib. In vivo IVIS images showed a remarkable emission enhancement (4.3-fold at 24 h and 7.3-fold at 36 h) in tumors from mice treated with palbociclib and intravenously injected with **S3**, whereas negligible signal was found in mice only treated with **S3** and in palbociclib-treated mice without **S3** administration. In good accordance, ex vivo IVIS images showed that fluorescence ascribed to NB was only observed in senescent tumors (17.6-fold enhancement) but not in control tumors or other organs. The performance in terms of selectivity and sensitivity makes **S3** an efficient on/off probe for the in vivo detection of senescence. We anticipate that this or similar probes will become essential tools to monitor treatment response and efficacy of senotherapies in a wide range of aged-related diseases.

### Acknowledgements

R.M. thanks financial support from the Spanish Government (RTI2018-100910-B-C41 and RTI2018-101599-B-C22 (MCUI/AEI/FEDER, UE)) and the Generalitat Valenciana (PROMETEO 2018/024). M.O. thanks the financial support from SAF2017-84689-R project and MINECO/AEI/FEDER, UE and the Generalitat Valenciana (PROMETEO/2019/065). B.L.-T. is grateful to the Spanish Ministry of Economy for her PhD grant. I.G. thanks her contract from IDM. J.F.-B. and M.A. thank the UPV for their postdoctoral fellowship.

### Conflict of interest

The authors declare no conflict of interest.

**Keywords:** in vivo detection · mesoporous nanoparticles · Nile blue · NIR probes · senescence

- [1] S. He, N. E. Sharpless, *Cell* **2017**, *169*, 1000–1011.
- [2] a) B. Lozano-Torres, A. Estepa-Fernández, M. Rovira, M. Orzáez, M. Serrano, R. Martínez-Máñez, F. Sancenón, *Nat. Rev. Chem.* **2019**, *3*, 426–441; b) D. Muñoz-Espín, M. Serrano, *Nat. Rev. Mol. Cell Biol.* **2014**, *15*, 482–496.
- [3] A. Hernandez-Segura, J. Nehme, M. Demaria, *Trends Cell Biol.* **2018**, *28*, 436–453.
- [4] D. J. Baker, B. G. Childs, M. Durik, M. E. Wijers, C. J. Sieben, J. A. Zhong, R. Saltness, K. B. Jeganathan, G. C. Verzosa, A. Pezeshki, K. Khazaie, J. D. Miller, J. M. van Deursen, *Nature* **2016**, *530*, 184–189.
- [5] A. Soto-Gamez, M. Demaria, *Drug Discovery Today* **2017**, *22*, 786–795.
- [6] J. L. Kirkland, T. Tchkonja, Y. Zhu, L. J. Niedernhofer, P. D. Robbins, *J. Am. Geriatr. Soc.* **2017**, *65*, 2297–2301.
- [7] L. J. Niedernhofer, P. D. Robbins, *Nat. Rev. Drug Discovery* **2018**, *17*, 377–377.
- [8] L. Hayflick, P. S. Moorhead, *Exp. Cell Res.* **1961**, *25*, 585–621.
- [9] R. Zhang, P. D. Adams, *Cell Cycle* **2007**, *6*, 784–789.
- [10] J. Campisi, *Cell* **2005**, *120*, 513–522.

- [11] G. P. Dimri, X. Lee, G. Basile, M. Acosta, G. Scott, C. Roskelley, E. E. Medrano, M. Linskens, I. Rubelj, O. Pereira-Smith, *Proc. Natl. Acad. Sci. USA* **1995**, *92*, 9363–9367.
- [12] B. Lozano-Torres, I. Galiana, M. Rovira, E. Garrido, S. Chaib, A. Bernardos, D. Muñoz-Espín, M. Serrano, R. Martínez-Máñez, F. Sancenón, *J. Am. Chem. Soc.* **2017**, *139*, 8808–8811.
- [13] D. Asanuma, M. Sakabe, M. Kamiya, K. Yamamoto, J. Hiratake, M. Ogawa, N. Kosaka, P. L. Choyke, T. Nagano, H. Kobayashi, Y. Urano, *Nat. Commun.* **2015**, *6*, 6463.
- [14] D. Muñoz-Espín, *Transl. Med. Aging* **2019**, *3*, 1–5.
- [15] A. E. Ekpenyong-Akiba, F. Canfarotta, H. B. Abd, M. Poblocka, M. Casulleras, L. Castilla-Vallmanya, G. Kocsis-Fodor, M. E. Kelly, J. Janus, M. Althubiti, E. Piletska, S. Piletskyc, S. Macip, *Nanoscale Horiz.* **2019**, *4*, 757–768.
- [16] a) S. Aliberti, G. Soler-Illia, O. Azzaroni, *Chem. Commun.* **2015**, *51*, 6050–6075; b) C. de la Torre, I. Casanova, G. Acosta, C. Coll, M. J. Moreno, F. Albericio, E. Aznar, R. Mangues, M. Royo, F. Sancenón, R. Martínez-Máñez, *Adv. Funct. Mater.* **2015**, *25*, 687–695.
- [17] a) A. Bernardos, E. Aznar, M. D. Marcos, R. Martínez-Máñez, F. Sancenón, J. Soto, J. M. Barat, P. Amorós, *Angew. Chem. Int. Ed.* **2009**, *48*, 5884–5887; *Angew. Chem.* **2009**, *121*, 5998–6001; b) A. Agostini, L. Mondragón, A. Bernardos, R. Martínez-Máñez, M. D. Marcos, F. Sancenón, J. Soto, A. Costero, C. Manguan-García, R. Perona, M. Moreno-Torres, R. Aparicio-Sanchís, J. R. Murguía, *Angew. Chem. Int. Ed.* **2012**, *51*, 10556–10560; *Angew. Chem.* **2012**, *124*, 10708–10712; c) D. Muñoz-Espín, M. Rovira, I. Galiana, C. Giménez, B. Lozano-Torres, M. Paez-Ribes, S. Llanos, S. Chaib, M. Muñoz-Martín, A. C. Ucero, G. Garaulet, F. Mulero, S. G. Dann, T. Van Arsdale, D. J. Shields, A. Bernardos, J. R. Murguía, R. Martínez-Máñez, M. Serrano, *EMBO Mol. Med.* **2018**, *10*, e9355.
- [18] J. Mérian, J. Gravier, F. Navarro, I. Texier, *Molecules* **2012**, *17*, 5564–5591.
- [19] X. Zhang, S. Bloch, W. Akers, S. Achilefu, *Curr. Prot. Cytom.* **2012**, *60*, 12.27.1–12.27.20.
- [20] W. Fu, C. Yan, Z. Guo, J. Zhang, H. Zhang, H. Tian, W.-H. Zhu, *J. Am. Chem. Soc.* **2019**, *141*, 3171–3177.
- [21] O. V. Ovchinnikov, A. V. Evtukhova, T. S. Kondratenko, M. S. Smirnov, V. Y. Khokhlov, O. V. Erina, *Vib. Spectrosc.* **2016**, *86*, 181–189.
- [22] a) E. Aznar, M. Oroval, J. R. Murguía, R. Martínez-Máñez, F. Sancenón, *Chem. Rev.* **2016**, *116*, 561–718; b) A. Llopis-Lorente, B. Lozano-Torres, A. Bernardos, R. Martínez-Máñez, F. Sancenón, *J. Mater. Chem. B* **2017**, *5*, 3069–3083; c) A. García-Fernández, E. Aznar, R. Martínez-Máñez, F. Sancenón, *Small* **2020**, *16*, 1902242.
- [23] a) V. Kozlovskaya, B. Xue, E. Kharlampieva, *Macromolecules* **2016**, *49*, 8373–8386; b) D. K. Mishra, R. Shandilya, P. K. Mishra, *Nanomedicine* **2018**, *14*, 2023–2050; c) F. Seidi, R. Jenjof, T. Phakkeeree, D. Crespy, *J. Controlled Release* **2018**, *284*, 188–212; d) W. Chen, S. Zhou, L. Ge, W. Wu, X. Jiang, *Biomacromolecules* **2018**, *19*, 1732–1745; e) M. Vázquez-González, I. Willner, *Langmuir* **2018**, *34*, 14692–14710; f) R. M. Farid, N. A. H. A. Youssef, A. A. Kassem, *Curr. Pharm. Des.* **2017**, *23*, 6613–6629; g) D. Lombardo, P. Calandra, D. Barreca, S. Magazu, M. A. Kiselev, *Nanomaterials* **2016**, *6*, 125; h) A. Bansal, Y. Zhang, *Acc. Chem. Res.* **2014**, *47*, 3052–3060; i) N. Kamaly, B. Yameen, J. Wu, O. C. Farokhzad, *Chem. Rev.* **2016**, *116*, 2602–2663.
- [24] B. G. Trewyn, I. I. Slowing, S. Giri, H.-T. Chen, V. S.-Y. Lin, *Acc. Chem. Res.* **2007**, *40*, 846–853.

Manuscript received: March 20, 2020

Accepted manuscript online: May 16, 2020

Version of record online: June 8, 2020